Intensity-Driven-Adaptive-Neighborhood Technique for POLSAR Parameters Estimation

Gabriel Vasile[1,2], Emmanuel Trouvé[1], Mihai Ciuc[2], Philippe Bolon[1] and Vasile Buzuloiu[2]

[1]: Laboratoire d'Informatique, Systèmes, Traitement de l'Information et de la Connaissance
Université de Savoie - ESIA - BP 806 - F-74016 Annecy Cedex - FRANCE
Tel: +33 450 096 548 - Fax: +33 450 096 559 - Email: {gabriel.vasile|emmanuel.trouve|philippe.bolon}@univ-savoie.fr

[2]: Laboratorul de Analiza si Prelucrarea Imaginilor (LAPI),
Catedra de Electronica Aplicata si Ingineria Informatiei, Universitatea *Politehnica* Bucuresti, Bucharest, ROMANIA
Tel: +4021 402 4683 - Fax: +4021 402 4821 - Email: {gvasile|mciuc|buzuloiu}@alpha.imag.pub.ro

Abstract

In this paper, a new method to estimate polarimetric coherency matrices and derive associated parameters is presented. For each pixel of the data set, an adaptive neighborhood is computed by a region growing technique driven exclusively by the intensity images. The three intensity images of the POLSAR acquisition are fused in the region growing process to ensure the stationarity hypothesis of the derived statistical population. Then, all pixels within the obtained adaptive neighborhood are, either complex averaged or estimated by the locally linear minimum mean–squared error (LLMMSE), to yield a feature preserving reliable estimate of the polarimetric coherency matrix. The target entropy–alpha–anisotropy decomposition is applied on the derived polarimetric coherency matrix. Using this decomposition, unsupervised classification for land applications by an iterative algorithm based on a complex Wishart density function is employed. The method has been tested on airborne polarimetric synthetic aperture radar images (Northumberland Strait costal area – Canadian Space Agency).

Keywords: SAR polarimetric imagery, coherency estimation, adaptive neighborhood.

1 Introduction

A synthetic aperture radar (SAR) system measures both amplitude and phase of the backscattered signal, producing one complex image for each recording. Polarimetric synthetic aperture radar (POLSAR) is an extension of the SAR imaging system, the sensors being able to emit and receive two polarizations, usually horizontal (H) and vertical (V). Four polarization configurations, usually denoted by HH, VV, HV and VH (according to the emitted and received polarization) are simultaneously available. Under the assumption of reciprocal symmetric backscattering, the HV and VH modes are fused and the resulting configuration is denoted by XX (monostatic case). Polarimetric acquisitions are usually represented in the Pauli basis and are fully characterized by the 3×3 polarimetric coherency matrix [1].

The information provided by SAR polarimetry allows the discrimination of different scattering mechanisms. The first characteristic decomposition of target coherency matrix for target scattering decomposition was proposed in [2]. The received signal can be split into a sum of three scattering contributions with orthogonal polarimetric signatures. The orthonormal eigenvectors of the Hermitian target coherency matrix are used for analyzing the eigenvector space. The dominant scattering mechanism is represented by the largest eigenvalue of the coherency matrix. In [1], Cloude and Pottiers introduced the target entropy and the $\alpha - \beta$ model by assigning to each eigenvector the corresponding coherent single scattering mechanism. Founded upon this decomposition, unsupervised classification for land applications was performed by an iterative algorithm based on complex Wishart density function [3].

In the framework of polarimetric interferometric SAR imagery, a spatially adaptive filtering method for improving the accuracy of the coherency estimation was introduced in [4]. Eight directional sub–windows are defined in order to locate the most homogeneous area inside the considered neighborhood. The sub–window selection procedure is driven by the average of the available span images of the interferometric pair. The pixels within the selected sub–window are used to yield the filtered covariance matrix, which is derived from the locally LLMMSE estimator of the 6×6 covariance matrix:

$$\widetilde{C}_{pol} = \overline{C}_{pol} + b(C_{pol} - \overline{C}_{pol}). \quad (1)$$

In *Eq. (1)*, $\overline{C}_{pol}$ stands for the average value of the POL–InSAR covariance matrix computed in the given sub–window, while $b \in [0, 1]$ is a locally–computed weight that measures the local data stationarity.

This paper presents a new spatially adaptive algorithm for coherency matrix estimation. Around each pixel, an adaptive neighborhood is formed using a region growing technique. The region growing algorithm is driven by all the available intensity images (the terms corresponding to the main diagonal of the roughly estimated coherency matrix). Pixels belonging to an adaptive "intensity–driven region" are more likely to respect the local stationarity hypothesis than pixels belonging to a squared fixed size window. Finally, the algorithm estimates the coherency matrix either by direct complex multilooking or from the locally linear minimum mean–squared error estimator. The two estimation techniques were tested using three different spatial supports: a fix–sized symmetric neighborhood (boxcar filter), directional nonsymmetric windows and the proposed adaptive neighborhood. The results of the method have been validated on C–band polarimetric interferometric SAR data (Northumberland Strait costal area – Canadian Space Agency).

2 Adaptive Neighborhood Estimation

The conventional filtering method performs a complex averaging over a fixed size sliding window estimating the polarimetric coherency matrix

$$[T] = E\{k_i k_i^{*T}\}, \tag{2}$$

where $E\{...\}$ denotes the expectation value and k_i is the coherent scattering vector in the Pauli basis. In this type of approach the number of pixels averaged may not be sufficient to reduce the estimation variance and the stationarity hypothesis is not always respected. The **A**daptive **N**eighborhood (AN) allows us to solve these problems by selecting a larger number of pixels which belong to the same statistical population as the filtered pixel.

In the proposed method, only the intensity information is used to decide upon the membership of the connex pixels to the AN. Small homogenous regions within all three intensity images correspond to ground areas with an homogenous cover, which respect the stationarity hypothesis requirement for the estimation of the complex correlation in *Eq. 2*. After initial complex multilooking a rough and noisy estimation of $[T]$ (3×3 matrix) is available. A multivariate vector is built containing only the elements of the main diagonal of $[T]$:

$$p(m,n) = \begin{bmatrix} [T]_{11}(m,n) \\ [T]_{22}(m,n) \\ [T]_{33}(m,n) \end{bmatrix} = \begin{bmatrix} p_1(m,n) \\ p_2(m,n) \\ p_3(m,n) \end{bmatrix}. \tag{3}$$

The algorithm for constructing the AN consists of four steps:

1. ***Rough estimation of the seed value***. The marginal median in the 3x3 centered neighborhood is used as the seed value $\widehat{p}(m,n)$.

2. ***Region growing***. The three distances corresponding to the three components of the multivariate vector p are merged in a single aggregation test:

$$\sum_{i=1}^{3} \frac{\|p_i(k,l) - \widehat{p_i}(m,n)\|}{\|\widehat{p_i}(m,n)\|} \leq 2\frac{\sigma_n}{\mu_n}. \tag{4}$$

   where μ_n and σ_n are the speckle mean and standard deviation. The variation coefficient σ_n/μ_n is a standard parameter in SAR imagery, which is constant in homogenous areas and equal to $1/\sqrt{L_{eq}}$, (L_{eq} is the equivalent number of looks resulting from the initial averaging). All the eight direct neighbors $p(k,l)$ of the seed are accepted inside the AN, provided they meet *Eq. 4*. Then, the same procedure is applied for all of the neighbors of the newly included pixels and so on. The region growing iterates in this manner, until either the number of the pixels already included in the AN exceeds a predefined upper limit N_{max} or none of the neighbors verify the test condition given by *Eq. 4*. The pixels which have already been tested, but not accepted inside the AN (called *background pixels* in the sequel) are stored in a separate list.

3. ***Refined estimation of the seed value***. A more reliable estimator of the unspeckled seed value is now obtained by averaging the intensity of the pixels included in this "strict" AN: $\overline{p}(m,n)$.

4. ***Reinspection of the background pixels***. The background pixels $p(o,p)$ of the list created in step 2 are tested again and aggregated in the AN, provided that they meet the "enlarged" test condition:

$$\sum_{i=1}^{3} \frac{\|p_i(o,p) - \overline{p_i}(m,n)\|}{\|\overline{p_i}(m,n)\|} \leq 6\frac{\sigma_n}{\mu_n}. \tag{5}$$

   The test is less restrictive, as the inclusion threshold is larger than the one used in the first step of region growing. The coefficients 2 and 6, in *Eq. 4* and *Eq. 5*, are set in order to accept respectively 50% and 95% of a Gamma distributed population.

Then, the proposed method recomputes the complex averaging over the largest possible neighborhood (without loosing stationarity). In the case of the POLSAR data set, the matrix $[T]$ from *Eq. 2* is estimated by replacing the ensemble average required by their definition, with a spatial average within the **I**ntensity **D**riven **A**daptive **N**eighborhood (IDAN):

$$T = \sum_{(k,l)\in AN(m,n)} k_i(k,l) k_i^{*T}(k,l), \tag{6}$$

A recent study presented in [5] investigates speckle noise effects over the physical information retrieved in POLSAR data by means of the $H/\alpha/A$ decomposition.

As the sample eigenvalues consist of asymptotically nonbiased estimators of the true eigenvalues, the minimum number of looks in order to neglect biases must be determined. The optimisation algorithm of the sample eigenvalues proposed in [5] does not succeed in correcting H with less than 81 looks and A values with less than 121 looks. The IDAN estimation provides such a high number of samples, while preserving stationarity and spatial resolution.

Depending on the desired POLSAR application, another refinement of the estimation method may be employed. The strong multilooking induced by IDAN may affect the properties of the polarimetric scattering signatures of the targets. In order to compensate these effects, a new technique which fuses the IDAN estimation and the LLMMSE from [4] is proposed (IDAN–LLMMSE). Instead of the directional windows, the previously constructed AN provides the necessary spatial support for the final LLMMSE estimation of the coherency matrix as:

$$\widetilde{T} = \overline{T}_{IDAN} + b(T - \overline{T}_{IDAN}). \quad (7)$$

$\overline{T}_{IDAN}$ represents the average value of the POLSAR coherency matrix computed in the obtained AN, while $b \in [0, 1]$ is the filtering weight which is computed as in [4], the AN pixels of all the three available POLSAR span images being averaged.

3 Results and discussion

To illustrate the performances of the IDAN filtering method presented in *Sec. 2*, results obtained with real airborne polarimetric SLC images are reported. The airborne data set was acquired in 2001 by the Environment Canada CV-580 SAR system. It represents a repeated pass fully polarimetric C-band (1.25 GHz) acquisition. The SLC spatial resolution is 4 m in range and 0.43 m azimuth. The target area is the Northumberland Strait off the Coast of New Brunswick, near Prince Edward Island, Canada. The 10-looks roughly estimated coherency matrix (Fig. 1) reveals different sea ice types: first year ice, leads and new forming ice [6]. Despite the initial multilooking, the equivalent number of looks estimated on one intensity image is $L_{est} = 1$.

The IDAN and IDAN–LLMMSE estimation algorithms are applied to improve the roughly estimated coherency matrix. Several filters are also applied for comparison purposes: **B**oxcar **F**ilter (BF) and **I**ntensity **D**riven **D**irectional **N**eighborhood (IDDN), with complex multilooking or with locally linear minimum mean–squared error estimation (BF–LLMMSE, IDDN–LLMMSE). The implemented IDDN algorithm is similar to the one presented in [4], with the only difference that the window selection is driven on the sum of the three available span POLSAR images (all the diagonal terms of the coherency matrix). The parameters used for POLSAR data IDAN

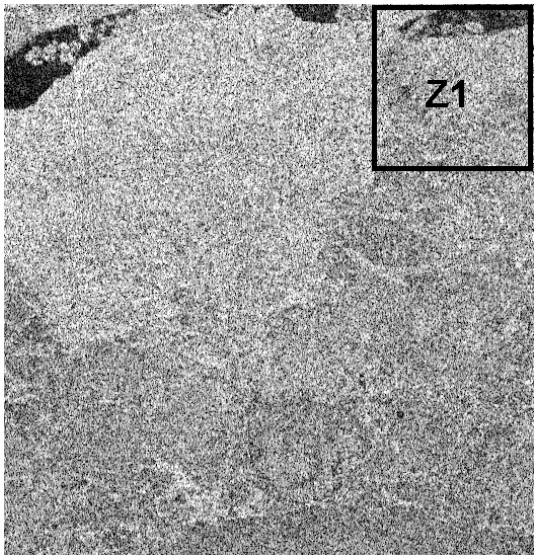

Figure 1: POLSAR initial data [523×544 pixels]: 10-looks T_{11} intensity.

filtering are: $N_{max} = 50$, $\sigma_{noise}/\mu_{noise} = 1$. In order to assure the compatibility of the BF, IDDN and IDAN, in terms of filtering amount, the size of the chosen BF centered neighborhood was 7×7.

In the case of nonadaptive filters, as the boxcar filter, the speckle reduction is always associated with strong edge–blurring effect (Fig. 2). The IDDN filter is more satisfactory than BF as the resulting edges are sharper. However, the fix size of the directional neighborhoods induces artifacts in the vicinity of thin details (smaller than the size of the neighborhoods). The BF–LLMMSE and IDDN–LLMMSE overcome these drawbacks, but the quality of the achieved noise reduction is decreased. The IDAN filter provides the best overall results: speckle is drastically reduced over homogenous area, whereas thin structures are preserved. Thanks to the large number of samples of the same distribution, used in performing the complex multilooking, the achieved speckle reduction is more important than in the case of the other spatial filters. A general remark for all the spatial filters is that the resulting filtered image has a patchy look, which is a known effect of purely spatial filtering. This effect is also observed for the IDAN. The IDAN-LLMMSE filter removes this effect, outperforming all the other filters from the visual point of view.

Fig. 3 presents the results of the Wishart classification using as input the coherency filtered by either IDAN or IDAN-LLMMSE. As expected, due to the strongest noise reduction on the homogenous area, the obtained results are much more regularized for the IDAN filtered coherency. The thin structures are very well defined in both cases. The IDAN classification reveals much more spatial information than the IDAN-LLMSE classification. It is

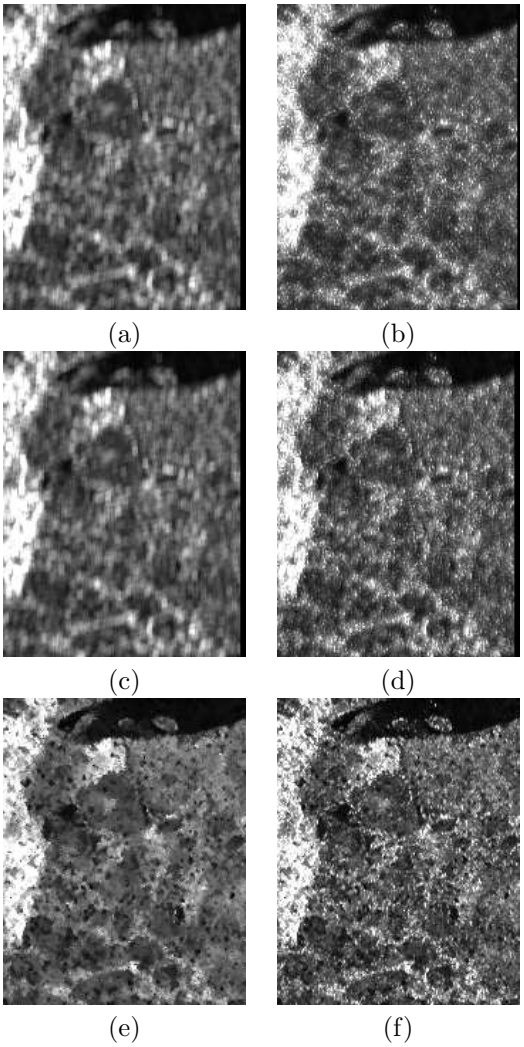

Figure 2: T_{11} intensity filtering results [171 × 216 pixels **Z1** of Fig. 1]: (a) BF, (b) BF–LLMMSE, (c) IDDN, (d) IDDN–LLMMSE, (e) IDAN, (f) IDAN–LLMMSE.

difficult to separate the different ice classes in *Fig.3-(b)*, whilst with IDAN (*Fig.3-(a)*) the ice classification is better defined. The sea area clearly appear in the upper right region of *Fig.3-(a)*.

4 Conclusion

A new method of filtering coherency matrices of polarimetric SAR data has been presented. The proposed filter uses adaptive neighborhoods as spatial support, derived with respect to the intensity information. All the available intensity images of the POLSAR data are combined in the region growing procedure, to ensure the stationarity assumption. The proposed filter recomputes the polarimetric coherency matrix, either by direct complex multilooking or from the locally linear minimum mean–squared error estimator of the roughly estimated coherency matrix.

The experimental results have proved that the noise is greatly reduced, while the contours and fine details are preserved and the blurring effect is avoided. Physical parameters of the scatterers (H, α, A) were computed and the influence of the proposed filtering method has been investigated. A final Wishart classification has been employed. All these features make this adaptive filtering algorithm a powerful tool for polarimetric data post-processing.

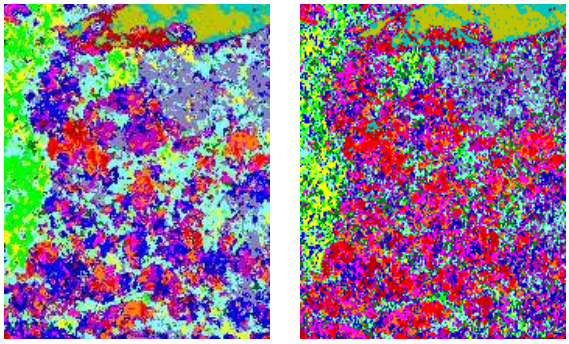

Figure 3: Wishart $H - \alpha$ classification of the filtered T_{11} intensity image [171 × 216 pixels]: (a) using IDAN, (b) using IDAN–LLMMSE.

Acknowledgments

The authors wish to thank the Canadian Space Agency and Environment Canada for providing the high resolution polarimetric SAR images.

References

[1] S.R. Cloude and E. Pottier. An entropy based classification scheme for land applications of polarimetric SAR. *IEEE Transactions on Geoscience and Remote Sensing*, 35(1):68–78, january 1997.

[2] S.R. Cloude. Group theory and polarization algebra. *OPTIK*, 75(1):26–36, 1986.

[3] J.S. Lee, M.R. Grunes, T.L. Ainsworth, D. Li-Jen, D.L. Schuler, and S.R. Cloude. Unsupervised classification using polarimetric decomposition and the complex Wishart classifier. *IEEE Transactions on Geoscience and Remote Sensing*, 37(5):2249–2258, september 1999.

[4] J.S. Lee, S.R. Cloude, K. Papathanassiou, M.R. Grunes, and I.H. Woodhouse. Speckle filtering and coherence estimation of polarimetric SAR interferometry data for forest applications. *IEEE Transactions on Geoscience and Remote Sensing*, 41(10):2254–2263, 2003.

[5] C. Lopez-Martinez and E. Pottier. Study of the speckle noise effects over the eigen decomposition of polarimetric SAR data. In *POLinSAR 2005 Workshop CD-ROM, Franscati, Italy*, 2005.

[6] M.R. Drinkwater, R. Kwok, E. Rignot, H. Israelsson, R.G. Onstott, and D.P. Winebrenner. *Potential Applications of Polarimetry to the Classification of Sea Ice, in F. Carsey.* AGU Geophysical Monograph, 68, Microwave Remote Sensing of Sea Ice edition, 1992.